Advanced Composites and Hybrid Materials (2023) 6:193
https://doi.org/10.1007/s42114-023-00764-8

RESEARCH

Directional transport of drug droplets based on structural and wettability gradients on antibacterial Janus wound plaster with hemostatic, antiextravasation, and prehealing properties

Jing Lin[1] · Zhen Yao[1] · Minmin Xiong[2] · Jin Lin[1] · Fei Hu[1] · Xinchuan Wei[1] · Songyin Huang[2]

Received: 11 August 2023 / Revised: 15 September 2023 / Accepted: 25 September 2023 / Published online: 21 October 2023

Abstract

The failure of wound healing is majorly attributed to uncontrolled bleeding and bacterial infections. However, developing a wound plaster that can stop bleeding, resist blood extravasation, and realize directional transportation of drugs to promote wound healing remains a significant challenge. Herein, a superhydrophilic/hydrophobic polyvinyl alcohol/chitosan/silver@Thermoplastic polyurethane (PVA/CS/Ag@TPU) Janus membrane with structural and wettability gradients is developed. In this newly developed membrane, water is absorbed from blood via the superhydrophilic layer, which is attached to the wound, and the charge interactions between platelets and the introduced chitosan (CS) promote blood clotting. The capillary pressure resistance ($\Delta p > 0$) of the superhydrophilic layer toward the hydrophobic layer prevents blood permeation, thereby reducing blood loss. The favorable Δp (< 0) of the membrane based on its structural and wettability gradients can realize the directional transportation of drugs that promote wound healing from the hydrophobic to the superhydrophilic layer. The incorporation of CS and silver endows the Janus membrane with intrinsic antibacterial properties (99.9%). The formation of the hydrated layer on the hydrophilic layer imparts a resisting effect, further endowing the membrane with antiadhesion and antibacterial properties. Experiments involving mice with full-thickness skin wounds revealed that the wound-healing rate increased from 87.65% to ~ 100% when the Janus membrane was loaded with the prehealing drug. Moreover, the dressing accelerated wound healing, regenerated epidermal and granulation tissues, promoted collagen formation, and reduced scar size. Thus, this gradient design strategy opens an avenue for the development of next-generation wound dressings.

Keywords Antibacterial · Hemostatic · Droplet transportation · Antiextravasation · Prehealing

1 Introduction

Uncontrolled bleeding and infections can lead to the failure of wound healing [1–6]. Uncontrolled traumatic and surgical bleeding constitutes a major cause of injury and death in war, accidents, and disasters [7, 8]. Excessive bleeding disrupts human hemodynamics [9], rendering individuals vulnerable to hypothermia, coagulopathy, infection, acidosis, multisystem organ failure, and death. Statistically, blood loss accounts for 35% of traumatic deaths, with 40% of hemorrhagic deaths occurring before hospital admission [10]. In addition, related bacterial infection is a serious problem that can cause injury and death [11]. Bacteria can grow and proliferate easily in the warm and humid environment of wound beds. In addition, the adhered and growing bacterial colonies can rapidly produce an extracellular polymer matrix on the wound surface, thereby imparting resistance toward the host immune system [12–14]. Bacterial infections prolong wound

Highlights
- An antibacterial Janus wound plaster with drug droplet directional transportation was developed.
- The structural and wettability gradients facilitate drug droplet directional transportation.
- This wound plaster exhibits hemostatic, antiextravasation, and prehealing muti-function.

✉ Jing Lin
linjin00112043@126.com; linjing@gzhu.edu.cn

✉ Songyin Huang
huangsy@mail.sysu.edu.cn

[1] School of Chemistry and Chemical Engineering, Guangzhou University, Guangzhou 510006, People's Republic of China

[2] Biotherapy Center, Sun Yat-Sen Memorial Hospital, Sun Yat-Sen University, Guangzhou, People's Republic of China

healing, leading to severe complications, such as bacteremia, septicemia, amputation, and even death [15, 16].

Unhealed wounds from traumatic accidents cause severe discomfort and vulnerability. Generally, wound healing is considered to comprise four stages: hemostasis, inflammation, proliferation, and remodeling [17, 18]. Therefore, an ideal wound dressing must support all the stages, consequently requiring hemostatic, antibacterial, cell proliferation, and regeneration properties.

Hemostasis is the first and most important stage of wound healing, and hence, it is vital to stop the bleeding in time. Substances that have been used to promote hemostasis in conventional wound dressings include chitosan, glue, aerogel, foam, hydrogel, and powder [19–27]. However, they are inconvenient owing to their need to be reapplied daily. Notably, a novel Janus membrane material with a wettability gradient that reduces blood loss, thus overcoming the aforementioned inconvenience, has recently emerged as a wound dressing [28–33]. Zhu et al. prepared a Janus hemostatic fabric by spraying paraffin wax on superhydrophilic gauze [34]. This Janus fabric effectively controlled bleeding and reduced blood loss by > 50% compared with ordinary fabric.

Wound protection against bacterial infection throughout the wound-healing process is also imperative [35–38]. Previous studies have reported that antibacterial fibrous wound dressings include, but are not limited to, intrinsic antibacterial, inorganic antibacterial agent–incorporated, antibiotic-loaded, and biological extract–containing dressings [39–41]. However, the latter two antibacterial dressings have some disadvantages: the overuse of antibiotics has resulted in the emergence of multidrug-resistant bacteria and the biological extract cannot maintain its biological activity.

Although eliminating wound infection is essential for wound healing, the subsequent cell proliferation and skin tissue remodeling are also important [42–45]. An external supply of wound-healing drugs is effective when the body exhibits poor internal repairing ability, including poor cell proliferation and skin tissue remodeling. Therefore, it is necessary to endow a wound dressing with excellent antibacterial and drug delivery properties to promote wound healing.

Recently, electrospinning technology has attracted considerable interest owing to its ability to prepare fibrous wound dressings with a large surface area, high porosity, and excellent gas permeability [46, 47]. Fibrous wound dressings mimic the native extracellular matrix, providing additional support for the adherence and migration of fibroblasts and keratinocytes, thereby promoting the regeneration of new tissues [48]. More importantly, the Janus structure gradient can be easily constructed through electrospinning technology with precisely controllable wettability and different pore structures in different layers. In addition, the construction of porous and breathable hemostatic wound plaster fiber membrane by electrospinning technology requires a series of biocompatible materials such as polyvinyl alcohol (PVA) or chitosan hydrogels and thermoplastic polyurethane (TPU) [49, 50], and nanomaterials with good antimicrobial property such as silver nanoparticle [51, 52].

This study proposes a strategy for the directional transportation of liquid drugs using a Janus plaster based on structural and wettability gradients. A PVA/CS/Ag@TPU Janus composite membrane was prepared via electrospinning technology with multifunctions including hemostasis, antiextravasation, antibacterial and bacterial antiadhesion properties, and directional transportation of drugs. Rapid hemostasis and good antiextravasation were realized via the wettability gradient of the Janus membrane, capillary pressure resistance (Δp), and coagulation effect of chitosan. Excellent antibacterial ability was obtained by combining the intrinsic antibacterial polymer and inorganic particles. A high level of bacterial antiadhesion was exhibited owing to the strong antibacterial ability, low underwater oil adhesion, and hydration layer formation of the membrane. The Janus composite membrane also allowed the directional transportation of drugs because of its Δp, which is based on its structural and wettability gradients. High wound-healing efficiency was achieved using the Janus plaster with prehealing drug droplet directional transportation. This study provides insights into the design of next-generation wound plaster.

2 Materials and methods

2.1 Materials

Thermoplastic polyurethane (TPU) was purchased from Dongguan Yisike Plastic Co. Chitosan ($M_w = 200{,}000$, with an 80% degree of deacetylation), polyvinyl alcohol ($M_w = 195{,}000$), N,N-dimethylformamide (DMF), acetic acid (99%), glutaraldehyde (50%), silver nitrate, hydrochloric acid (HCl), sodium chloride (NaCl), anhydrous calcium chloride ($CaCl_2$), sodium hydroxide (NaOH), and dichloroethane were obtained from Shanghai Macklin Biochemical Co., Ltd. Trisodium citrate ($Na_3C_6H_5O_7$) was supplied by Sinopharm Chemical Reagent Co., Ltd. Sodium borohydride ($NaBH_4$) was procured from the Tianjin Damao Chemical Reagent Factory. All reagents were of analytically pure grade and were used directly without further purification. Anticoagulant rabbit blood (12 wt%) sodium citrate was purchased from Henan Yuechi Biotechnology Co., Ltd. Medical gauze and medical tape were acquired from Haishihainuo Bio-engineering Co., Ltd. The prehealing liquid drug was obtained from Chengdu Chaoji Technology Co., Ltd. The polytetrafluoroethylene tube was supplied by Sanniu Electronic Material Co., Ltd. *Staphylococcus aureus* [CMCC(B) 26003], *Escherichia coli* [CMCC(B) 44102],

and phosphate-buffered saline (PBS) were obtained from the Guangdong Institute. Nutrient agar and nutrient broth were purchased from Sigma-Aldrich. A live/dead Baclight bacterial viability kit was purchased from Invitrogen (Carlsbad, CA, USA). The medical drug used to promote wound healing was purchased from Chengdu Chaoji Technology Co., Ltd.

2.2 Synthesis of triangular silver nanoprisms

Triangular silver nanoprisms were prepared via the photoinduced method [53, 54]. In brief, 250 µL silver nitrate ($AgNO_3$) (10 mmol/L) and 250 µL $Na_3C_6H_5O_7$ (10 mmol/L) were added to 24.25 mL ultrapure water in a beaker, rapidly and vigorously stirred using a magnetic stirrer for 10 min to ensure complete mixing of $AgNO_3$ and $Na_3C_6H_5O_7$. Subsequently, 250 µL of a mixture of $NaBH_4$ (8 mmol/L) and NaOH (0.125 mol/L) was added dropwise to produce a bright yellow silver seed solution. After continuous stirring for 2 min, the solution was exposed to light from above using a 120 W sodium lamp, and continuous stirring was performed under illumination. After 3.5 h of illumination, the reaction was terminated, and a solution containing blue triangular silver nanoprisms was obtained.

2.3 Preparation of the Janus composite membranes

As depicted in Fig. 1, Janus composite membranes (PVA/CS/Ag@TPU and PVA/CS@TPU) were prepared via the following procedures. Chitosan (0.3 g) was dissolved in a 3 wt% acetic acid (9.7 g) solution to obtain a 3 wt% chitosan solution. PVA (0.9 g) was dissolved in deionized water (9.1 g) to obtain a 9 wt% PVA solution. The PVA/CS/Ag blend solution was obtained by mixing the 3 wt% chitosan (6.3 g), 9 wt% PVA (2.7 g), and silver nanoprism solutions (1 g). A PVA/CS blend solution was also obtained by mixing

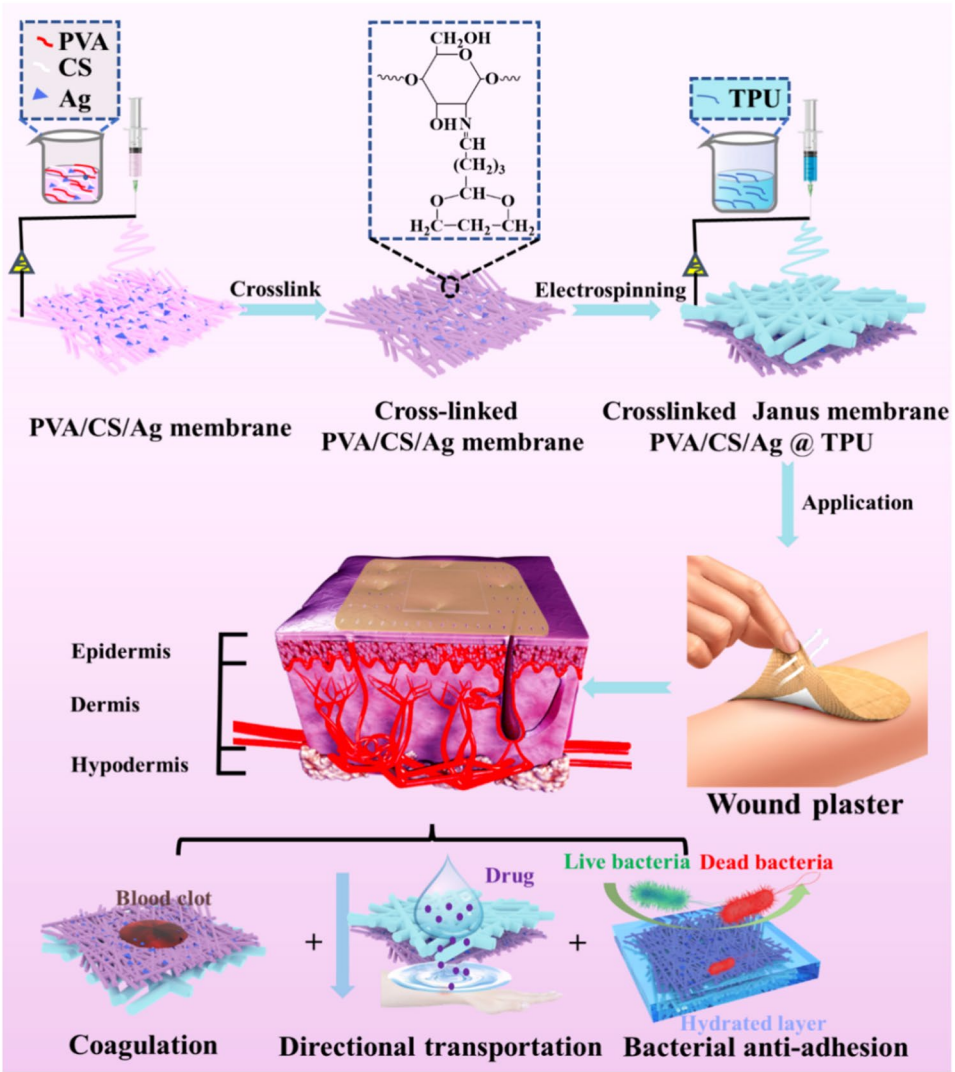

Fig. 1 Schematic diagram of the preparation process of Janus PVA/CS/Ag@TPU composite membrane and its wound plaster application

3 wt% CS (6.3 g) and 9 wt% PVA (2.7 g). TPU (1.5 g) was added to DMF (8.5 g) to obtain a 15 wt% TPU solution. For the PVA/CS/Ag@TPU Janus composite membrane, the PVA/CS/Ag hydrophilic layer was produced via electrospinning the PVA/CS/Ag solution using an electrospinning machine (HZ-11, Shandong Huizhi electrospinning, Co., Ltd., China). A hydrophobic TPU layer was subsequently produced by electrospinning a TPU solution on the hydrophilic layer to obtain a PVA/CS/Ag@TPU Janus composite membrane. For the PVA/CS@TPU Janus composite membrane, the PVA/CS hydrophilic layer was produced by electrospinning a PVA/CS solution. The hydrophobic TPU layer was then electrospun on the hydrophilic layer to obtain a PVA/CS@TPU Janus composite membrane. The PVA hydrophilic membrane was produced by electrospinning a PVA solution. The electrospinning parameters were as follows: the abovementioned solution, apart from TPU, was added to a 20-mL injection syringe using a 23-G metal needle at 0.6 mL/h, and a high direct current voltage of 26 kV was applied to each needle tip. The TPU solution was pumped at 2 mL/h, and a high direct current voltage of 12 kV was applied to each needle tip. The electrospun membranes were collected on the aluminized paper of the drum setup at a rotating speed of 100 rpm. The distance between the needle tips and drum setup was 15 cm. The stability of the hydrophilic electrospun membranes was improved via crosslinking using glutaraldehyde vapors generated from 10 mL 25 wt% glutaraldehyde solution in a vacuum drying oven at 60 °C for 10 h.

2.4 Characterization and measurements

The characteristic absorption peaks of the triangular silver nanoprisms were measured using an ultraviolet–visible spectrometer (UV, UV-2550, Nanjing Kejie Analytical Instrument Co., LTD, China). The morphology, dispersion, and particle size of the triangular silver nanoprisms were characterized via transmission electron microscopy (TEM, FEI Tecnai F20, FEI, USA). The micromorphology of the Janus composite membrane was observed via field emission scanning electron microscopy (FESEM, JSM-7001F, JEOL, Japan). One hundred fibers were selected randomly and measured using ImageJ software to calculate the mean fiber diameter. Fourier-transform infrared (FT-IR) spectroscopy was performed using an FT-IR spectrometer (Thermo Scientific Nicolet iS5, USA). The elemental components of the Janus composite membrane surface were examined using X-ray photoelectron spectroscopy (Thermo ESCALAB 250XI, USA). The element distribution on the Janus composite membrane surface was analyzed using energy dispersion X-ray spectroscopy (EDX, Model Inca400, Oxford Instruments, UK). The crystal structures of the Janus composite membrane were characterized via X-ray diffraction (Ultima VI, Rigaku, Japan). The mean pore size of the fibers was measured using a capillary pore-flow apparatus (CFP-1500AE, PMI, USA). The silver content of the CS/PVA/Ag membrane was measured using inductively coupled plasma optical emission spectrometry (PerkinElmer 8300, USA). The water contact angle in air and the oil contact angle underwater were measured using a contact angle–measuring instrument (OCA40-Micro, Date physics, Germany). Underwater oil adhesion was measured using an interfacial tension tester (K100, KRUSS, Germany). The zeta potential was determined using a zeta potential analyzer (90Plus PALS, Brookhaven Instruments Corporation, USA). Fluorescence staining was performed to evaluate the number bacterial distribution in the feed and filtrate. The dead and live states of bacteria after dyeing were observed via fluorescence microscopy (Olympus BX51, Japan), and the excitation/emission wavelength was 440–480/515–540 nm.

2.5 Evaluation of the blood coagulation potential

The blood coagulation potential of the Janus composite membrane was evaluated by adding 10 µL distilled water dropwise on the surface of the hydrophilic and hydrophobic membranes, respectively, and the absorption of the droplets was observed. Subsequently, 10 µL anticoagulant rabbit blood with 15 wt% sodium citrate was added dropwise to the hydrophilic surface of the Janus composite membrane. The clots generated on the hydrophilic and hydrophobic surfaces of the Janus membrane were photographed.

2.6 Liquid absorption

First, a salt solution closely resembling the composition of body fluid was prepared. The solution comprised sodium chloride (0.8298, w/v) and calcium chloride (0.0368%, w/v) solutions. The Janus composite membrane was completely immersed in a salt solution and cultured for 0, 10, and 30 min, and 1 and 2 h. Excess liquid was removed, and the sample was weighed to assess the absorption ratio. Each measurement was repeated thrice. The absorption ratio was calculated using Eq. 1.

$$Absorption\ ratio(\%) = \frac{M_1 - M_0}{M_0} \times 100 \quad (1)$$

where M_0 and M_1 represent the weight of dry and wet Janus composite membranes, respectively.

2.7 In vitro blood coagulation test

The samples (medical gauze as the control, PVA membrane, and Janus composite membrane) were sectioned into circles with a 1-cm diameter and preheated in a glass plastic Petri

dish (37 °C in a water bath). Anticoagulant rabbit blood containing 15 wt% sodium citrate was used for the coagulation test. The anticoagulant rabbit blood was mixed with 0.2 M calcium chloride at a 10:1 volume ratio to induce blood coagulation, and 25 μL blood was immediately dropped onto the center of the circular samples of the medical gauze, PVA membrane, and Janus composite membrane (hydrophilic layer upward). As a control, 25 μL blood was placed in an empty Petri dish without the samples. The blood on the different samples was coagulated at 37 °C for 5 min, and 10 mL deionized water was gently added to the Petri dishes to terminate the coagulation without disturbing the clots. The uncoagulated red blood cells (red blood cells not trapped in the blood clots) were hemolyzed, and hemoglobin was released into the water. The optical density (OD) of the hemoglobin solution was measured at 540 nm using a spectrophotometer (UV-2550, Nanjing Kejie Analytical Instrument Co. Ltd., China). Each measurement using the same batch of blood was repeated thrice. The hemoglobin content in water at the clotting time (t) and hemoglobin content in water was calculated using Eq. 2.

$$Hemoglobin\ content(g/L) = OD \times 367.7 \tag{2}$$

where OD represents the absorbance value of the sample.

The blood absorption capacity was measured by completely immersing the samples (medical gauze, PVA membrane, and Janus composite membrane) in the anticoagulant rabbit blood (15 wt% sodium citrate). Blood absorption was calculated using Eq. 3.

$$Blood\ absorption(\%) = \frac{M_{1\_}M_0}{M_0} \times 100 \tag{3}$$

where M_0 represents the weight of the dry medical gauze, PVA film, or Janus composite film, and M_1 represents the weight of the samples after absorbing the anticoagulant rabbit blood. The clotting time was measured by adding 2 mL of anticoagulant rabbit blood to test tubes containing 20 mg of medical gauze (control), PVA membrane, and Janus composite membrane. Subsequently, 60 μL of calcium chloride (0.25 mol/L) solution was added to the test tube. The tube was tilted every 15 s, and the time when there was no blood flow was recorded. Each measurement was repeated three times.

2.8 Hemostasis test of in vitro vascular injury model

An opening (5 × 8 mm) was made on the polytetrafluoroethylene tube (inside diameter: 10 mm) to simulate the vascular tissue of the wound. The opening was covered with medical gauze or Janus composite film (the hydrophilic layer adhered to the opening, and the hydrophobic layer faced outward) and fixed with medical tape. The entire vessel model was attached to a pre-weighed Petri dish. A 2-mL sample of anticoagulant rabbit blood (mixed with calcium chloride to cause clotting) was added to each tube. After the tube was removed, the increased weight of the Petri dish was recorded as the amount of blood lost in this vascular model. Each measurement was repeated three times.

2.9 Water droplet directional transportation

Blue ink was used as a test droplet to characterize the liquid directional transport capability of the Janus membrane. Droplets of 25, 50, or 100 μL were placed on the hydrophobic or superhydrophilic layer surface of the Janus composite membrane (a square with a side length of 3.5 cm). The diffusion process of the ink on the hydrophobic and hydrophilic layer surfaces of the Janus composite membranes was recorded by video. The relationship between the diffusion diameters and the time when droplets with different volumes were dropped onto the hydrophobic and hydrophilic layer surfaces of the Janus composite membranes were measured.

2.10 Prehealing drug droplets directional transportation

The directional transportation of prehealing drug droplets on the Janus wound plaster was investigated. A drop of the prehealing drug was placed on the hydrophobic layer, and the transportation performance of the prehealing drug was observed. The prehealing drug transport capacity of the Janus composite membrane was measured by sectioning the sample into a square with a side length of 2.3 cm and attaching it to the inner side of a funnel filter. A 2-mL sample of the prehealing drug was fed into the funnel filter. The filtered drug liquid that passed through the Janus composite membrane was collected. A 1-mL sample of filtered drug liquid was collected and placed into a drying oven until the drug liquid had evaporated. The weights of the prehealing drug were calculated before and after drying, and the solid content was calculated using Eq. 4.

$$Solid\ content(\%) = \frac{M_1}{M_0} \times 100 \tag{4}$$

where M_0 and M_1 represent the weights of the prehealing drug before and after drying, respectively.

2.11 Antibacterial test and live/dead bacteria fluorescence staining

The antibacterial ability of the samples was evaluated using *E. coli* (gram-negative bacteria) and *S. aureus* (gram-positive bacteria). In brief, 50 mL sterilized PBS and 1 mL 10^7 CFU/mL bacterial suspension were placed

in a conical flask. Subsequently, 20 mg PVA/CS@TPU or PVA/CS/Ag@TPU samples were added, and the flask was shake-incubated at 37 °C for 8 h at 180 rpm. A test with no sample was used as the control. Following cultivation, the bacterial solution was diluted tenfold. A 100-μL sample of the bacterial solution was spread over the surface of solid nutrient agar in a Petri dish, and the dish was incubated at 37 °C for 12 h. The experiment was repeated thrice for each group. The antibacterial rate (%) was calculated using Eq. 5.

$$\text{Antibacterial rate}(\%) = \frac{N_2 - N_1}{N_1} \times 100 \quad (5)$$

where N_1 and N_2 represent the number of colonies for the control and after sample incubation, respectively.

To assess the live/dead state of the bacteria following cultivation, 100 μL bacterial suspension was spread on a microscope slide, and 25 μL fresh SYTO9/PI fluorescent stain solution was added to it dropwise. Then, the slide was covered with a glass coverslip. The bacteria were thoroughly stained in the dark for 15 min, and the live/dead states of the bacteria were observed under fluorescence microscopy.

2.12 Bacterial antiadhesion test and live/dead bacteria fluorescence staining

The bacterial antiadhesion properties of the samples were evaluated using a slightly modified version of a methodology reported by Lin et al. [55–61]. Briefly, the PVA and Janus membranes were sectioned into 1-cm diameter disks and separately placed in test tubes where the hydrophilic layer of the Janus membrane was placed toward the mouth of the tube. Subsequently, 100 μL 10^7 CFU/mL bacterial suspension was added dropwise to the samples and into the test tube not containing a sample (control). Then, the tubes were incubated under static conditions for 1 h at 37 °C. Following incubation for 1 h, 10 mL PBS was added to each test tube, and the tubes were further incubated in an incubation shaker at 180 rpm for 30 min at 37 °C. following incubation, the bacterial suspension was diluted 10 times. Next, 100 μL diluted bacterial solution was spread onto the surface of solid nutrient agar in a Petri dish, which was incubated at 37 °C for 12 h. The experiment was repeated thrice for each group. The colony count following incubation was measured to determine the extent of the bacterial antiadhesion of the membrane.

Following the bacterial antiadhesion test, the live/dead state of the bacteria was observed by adopting the same bacterial fluorescence-staining method described in Section 2.11.

2.13 Animal experiments

Male C57BL/6 mice, weighing ~ 20 g, were divided into four groups before surgery. The mice were anesthetized with an intraperitoneal injection of 1 wt% sodium pentobarbital. The back area was shaved and disinfected with 70 wt% alcohol and covered with gauze to isolate the skin from the external environment. A hole punch was used to produce a circular, full-thickness wound (diameter of 7 mm) on the back of each mouse. The wound was treated with the following wound dressings: medical gauze (control), PVA membrane, Janus composite membrane (hydrophilic layer stuck to the wound), and Janus composite membrane (hydrophilic layer stuck to the wound), following which 10 drops of the prehealing drug liquid was added. The wound dressing was changed every 2 days. On days 4, 7, and 10, the wounds were photographed using a digital camera, and the mice were weighed. The percentage of healed wound area was calculated using Eq. 6.

$$\textit{Wound area}(\%) = \frac{S_2}{S_1} \times 100 \quad (6)$$

where S_1 represents the original wound area (day 0), and S_2 represents the wound area following treatment at different times.

2.14 Histological and immunofluorescence staining

For histological and immunofluorescence analyses, the wound tissues of the mice were sliced into 4-μm sections on days 4, 7, and 10, respectively. Subsequently, the tissue sections were fixed using 4 wt% paraformaldehyde and embedded in paraffin. Finally, they were subjected to hematoxylin and eosin (H&E), Masson trichromatic, and immunofluorescence staining. The stained sections were imaged and analyzed, and quantitative analysis was performed using ImageJ software.

2.15 Statistical analysis

The quantified results were reported as the mean ± standard deviation. Data analysis was performed on the histological and immunohistochemical tissues. The differences between different groups were assessed using Student's *t*-test, and p values of < 0.05 were considered significant.

2.16 Mechanical performance measurement of wound plaster

Tensile testing of wound plaster was performed using a universal testing machine (AG-1S Shimadzu, Schimadzu Corp., Tokyo, Japan), the sample was cut into strip with dimension similar to that of commercially available hemostatic strip, its thickness was measured using a digital calliper. The tensile

strength and elongation at break could be obtained after performing tensile testing.

3 Results and discussion

3.1 Characterization of superhydrophilic/hydrophobic Janus membranes with structural and wettability gradients

A cross-section of the Janus composite membrane revealed that the hydrophilic layer was thicker than the hydrophobic layer (~250 vs. ~25 µm) alongside a clear boundary between the two layers and good bonding between them (Fig. 2a). A higher magnification image showed differences in the fiber and pore sizes between the two layers. The nanofiber surface of the superhydrophilic layer (Fig. 2c) was smoother than that of the hydrophobic layer (Fig. 2b), and the average diameter of the hydrophilic layer nanofiber (138 nm) was considerably smaller than that of the hydrophobic layer nanofiber (1,116 nm) (Fig. 2d). Similarly, the pore size of the hydrophilic layer (PVA/CS/Ag) (223.4 nm) was substantially smaller than that of the hydrophobic layer (2,191 nm) (Fig. 2e), and a gradient of morphologically controllable pore size was established between the two layers, which was conducive to directional transportation of the prehealing drug liquid [62–64]. Thus, a structural gradient from large to small fiber size of the membrane channels from the

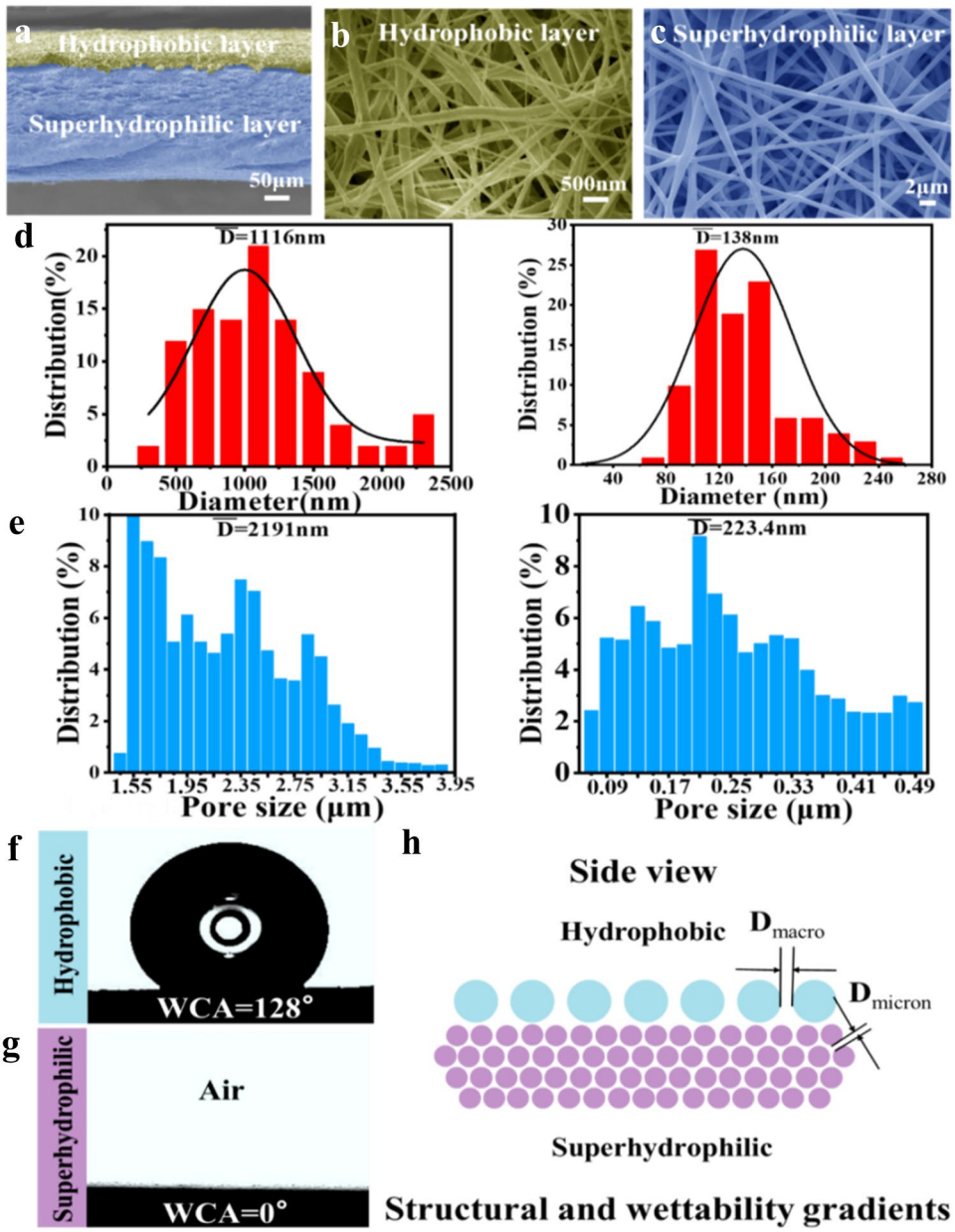

Fig. 2 Field emission scanning electron microscopy (FESEM) images of the **a** cross-section of the Janus composite membrane and its **b** superhydrophilic (PVA/CS/Ag) and **c** hydrophobic layers (TPU). The fiber diameter distribution of the **d** superhydrophilic (PVA/CS/Ag) (left) and hydrophobic layers (TPU) (right). The pore size distribution of **e** the superhydrophilic (PVA/CS/Ag) and hydrophobic layer (TPU). Water contact angles (WCA) of the **f** hydrophobic layer (TPU) and **g** superhydrophilic layer (PVA/CS/Ag). **h** Schematic illustration of the Janus composite membranes with structural and wettability gradients

hydrophobic to superhydrophilic layers was created, which provided sufficient conditions for the directional transportation of droplets through the membrane. FESEM-EDX confirmed that the expected elements were well distributed on the PVA/CS/Ag or TPU composite membranes (Fig. S1).

The surface wettability of the Janus composite membrane surfaces exhibited substantial differences, with water contact angles (WCAs) of 128° (Fig. 2f) and 0° (Fig. 2g) on the hydrophobic and superhydrophilic surfaces, respectively. The results demonstrated that the Janus membrane exhibited structural and wettability gradients.

3.2 In vitro hemostasis of Janus composite membrane based on structural and wettability gradients

When 10 μL anticoagulant rabbit blood (containing 12% sodium citrate) was added dropwise to the superhydrophilic layer of the Janus composite membrane, as shown in Fig. 3a, the anticoagulant blood was slowly absorbed by the superhydrophilic layer and then condensed into black clots. Furthermore, no blood exuded from the surface of the hydrophobic layer, indicating that the hydrophobic layer plays a role in antiextravasation. The coagulation property is closely associated with surface wettability, volume and weight of the samples, and anticoagulant and calcium chloride contents in the blood. The blood absorption capacity of the samples was further evaluated. High blood absorption capacity is suitable for stopping large amounts of bleeding. The blood absorption capacity of the Janus composite membrane was 10.21 times its weight, which was higher than that of the PVA membrane (9.32 times) and medical gauze (7.13 times) (Fig. 3b). The blood absorption capacity of the Janus membrane was higher than that of PVA because the hydrophilic fiber of the Janus membrane absorbs water from the blood, and chitosan coagulates blood.

The in vitro hemostasis speed of the samples was evaluated by determining the coagulation time. When the Janus composite membrane group was completely coagulated, some blood still flowed in the PVA membrane group. More than half the blood in the medical gauze had not completely coagulated (Fig. 3c). The blood coagulation speed results (Fig. 3d) revealed that the coagulation time of the Janus composite membrane (403 ± 10 s) was shorter than that of medical gauze (511 ± 12 s) and PVA membrane (460 ± 14 s), indicating that the Janus composite membrane has advantages in promoting coagulation rapidly owing to the water absorption of the hydrophilic layer from the blood and the positive charge of chitosan, which synergizes with the negative charge of platelets to accelerate hemostasis. The coagulation capacity of the samples was evaluated by measuring the concentration of hemoglobin released by uncoagulated blood using a dynamic whole-blood coagulation model (Fig. S2a). Human blood coagulation was stimulated (Fig. 3e) by placing the samples into a Petri dish at 37 °C, and anticoagulant blood that contained calcium chloride was added dropwise to the samples. After 5 min, 10 mL water was slowly added from the edge of the Petri dish. Uncoagulated blood released hemoglobin into the water. In the control group (medical gauze), the water around the medical gauze turned red owing to uncoagulated blood, indicating that the coagulation ability of the medical gauze was low. In the PVA membrane group, the water turned slightly red. Conversely, the water around the Janus composite membrane (superhydrophilic upward) remained almost transparent, suggesting that the blood was almost entirely coagulated, and the Janus composite membrane had a coagulation effect.

The hemoglobin concentration of the uncoagulated blood of the different samples was quantitatively analyzed, and the hemoglobin concentration (g/L) of 25 μL blood was considered a reference. A lower hemoglobin concentration is associated with better coagulation ability. Compared with the control (102.1 g/L, 14.98%) and PVA (86.1 g/L, 28.3%) groups, the hemoglobin concentration of the Janus composite membrane (46.5 g/L, 61.24%) was the lowest (Fig. 3f), indicating optimal coagulation ability. The vascular injury bleeding model was used to measure the hemostatic effect of the Janus membrane in massive bleeding emergencies. A hole was made on the side of polytetrafluoroethylene hoses to simulate a wound similar to that on blood vessels. The wound was covered with medical gauze and the Janus composite membrane (superhydrophilic layer stuck to the wound and the hydrophobic layer facing outward) and fixed with medical tape. Blood containing calcium chloride was then injected into the hole (Fig. 3g). The blood loss in the Janus composite membrane group was 0 g, with no blood exudation (Fig. 3h). Conversely, the average blood loss in the medical gauze group was $94.3\% \pm 2.2\%$. These results indicate that the Janus composite membrane exhibits excellent hemostasis and antiextravasation properties.

The absorption rate of the Janus membrane per unit weight increased with time (Fig. S2b), which was conducive to hemostasis. Therefore, the superhydrophilic layer absorbed water from blood, while the hydrophobic layer prevented blood permeation. The reason for this is that the PVA/CS/Ag layer is superhydrophilic. The chitosan in the superhydrophilic layer plays an important role in blood coagulation because the zeta potential of the chitosan solution (3 wt%) is positive (56.6 mV) (Fig. S2c). A positive charge can have electrostatic interactions with the negatively charged platelets in the blood [65], causing platelet aggregation, resulting in blood coagulation and promoting hemostasis.

The intrinsic clotting mechanism of the Janus composite membrane was analyzed (Fig. 3i). The water in the blood can be rapidly absorbed by the superhydrophilic layer of the Janus composite membrane, leading to the

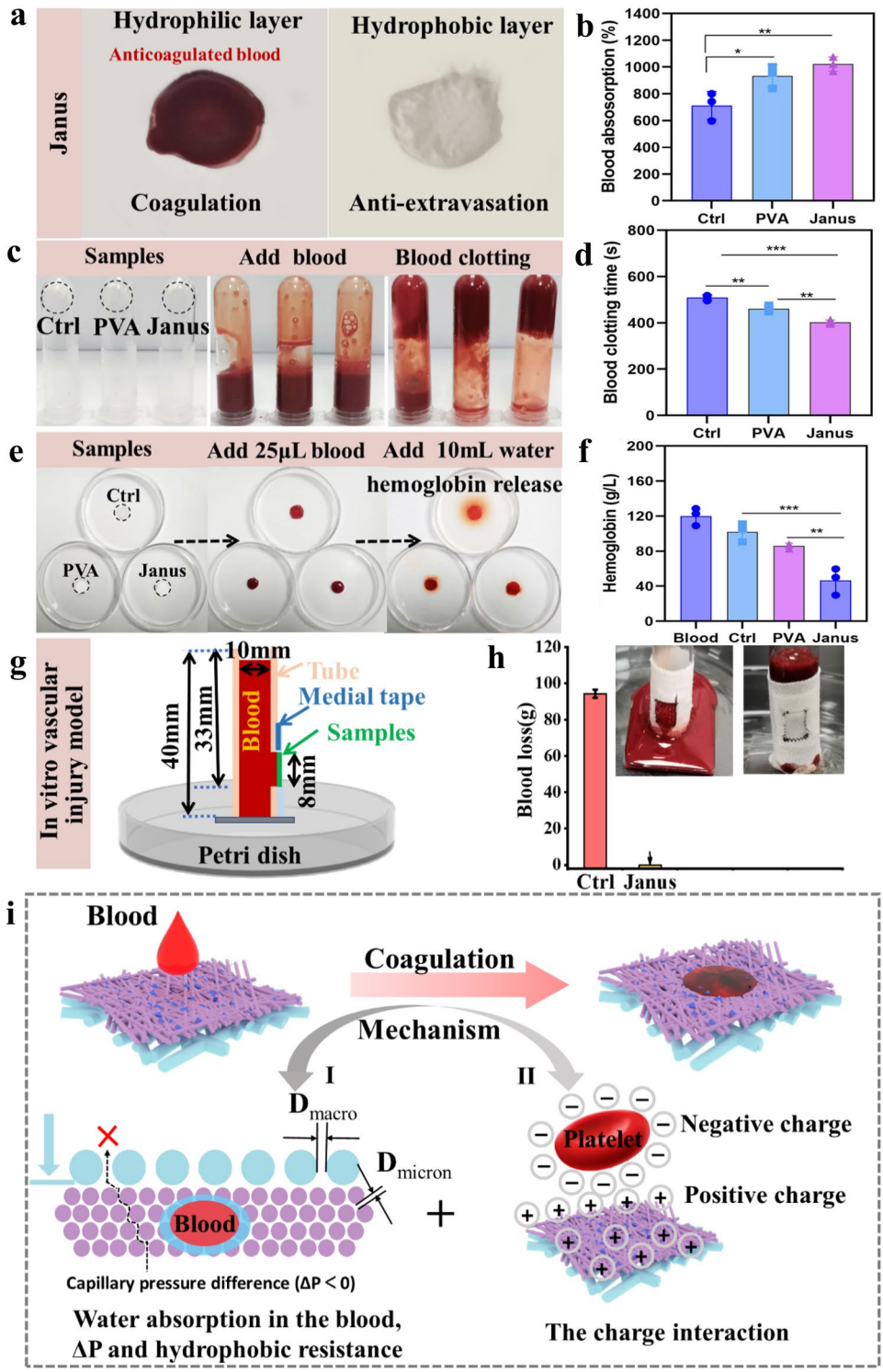

Fig. 3 Blood coagulation photograph of **a** superhydrophilic (CS/PVA/Ag) and antiextravasation photograph of **b** hydrophobic layers (TPU) of the Janus composite membrane when blood was dropped onto the superhydrophilic layer (CS/PVA/Ag). **b** Blood absorption capacity of the samples. **c** Photographs of the blood clotting formation process. **d** Blood clotting time of the samples. **e** Photographs of a dynamic whole-blood clotting model were used to evaluate the in vitro hemostatic properties. **f** Concentration of hemoglobin not trapped in the clots of the samples. **g** Vascular injury model. **h** Blood loss with medical gauze and Janus composite membrane in the in vitro vascular injury model. **i** Schematic diagram of the coagulation mechanism of the Janus composite membrane. Statistical diagrams represent mean ± SD of three separate experiments and significance was determined by one-way ANOVA, $*p < 0.05$, $**p < 0.01$, $***p < 0.001$

aggregation of the red blood cells, platelets, and clotting factor. Therefore, the absorption of water is beneficial for blood coagulation. When blood arrives at the interface of the superhydrophilic/hydrophobic layers, a capillary pressure difference (ΔP) is generated. ΔP was calculated using Eq. 7.

$$\Delta P = P_{L1} - P_{L2} = \frac{4\gamma cos\theta_2}{D_2} - \frac{4\gamma cos\theta_1}{D_1} \quad (7)$$

where D_1 and D_2 represent the diameters of the macro- and micron-sized pores and θ_1 (128°) and θ_2 (0°) are the corresponding WCAs of the inner surface of the capillary

pores, respectively. The capillary pressure of the micron-sized pores (P_{L1}) was considerably larger than that of the macro-sized pores (P_{L2}). Thus, ΔP (>0) plays a key role in the resisting force that prevents the blood from directly contacting the superhydrophilic layer and permeating into the hydrophobic layer. During the process of blood absorption from the wound into the hydrophilic layer, the positively charged chitosan in the superhydrophilic (PVA/CS/Ag) layers bind to the negatively charged platelets, and the latter accumulate to promote hemostasis. Therefore, the potential coagulation mechanism of the Janus composite membrane was due to the water absorbed by the superhydrophilic layer, coagulation effect of chitosan, and capillary pressure difference resistance (ΔP), which prevented blood extravasation.

3.3 Directional transportation of drugs in the Janus composite membrane

The Janus composite membrane with a designed wettability gradient is useful for the regular administration of drugs by adding drug droplets to the surface of the hydrophobic layer to promote wound healing after hemostasis. A prehealing drug liquid was considered the research object. The drug liquid added dropwise to the hydrophobic layer of the wound plaster was initially spherical (I), which then collapsed and was transported from the hydrophobic layer to the superhydrophilic layer (II), further penetrating and diffusing downward (III) until the droplet on the surface of the hydrophobic layer completely penetrated the dressing (IV) (Fig. 4a). The drug liquid completed the directional transportation from the hydrophobic to the superhydrophilic layer. To verify that the Janus composite membrane exhibited no blocking effect on the drug liquid, the transported drug liquid from the hydrophobic to the superhydrophilic layer was collected, and the solid content of the drug liquid before and after transportation was measured (Fig. S3). The solid content of the original drug liquid (2.47%) was slightly lower than that of the drug liquid following transportation through the Janus composite membrane (2.66%). This result was attributed to the hydrophilic layer of the Janus membrane absorbing some water from the drug liquid. For further observation and analysis of the directional transportation within the Janus composite membrane, ink was adopted, as shown in Fig. 4b. The ink droplet on the hydrophobic layer began to collapse after 5 s. After 15 s, the wet area of the superhydrophilic layer was larger than that of the hydrophobic layer, and the wet area gradually increased until 65 s had elapsed. This suggests that the droplets permeate and diffuse into the superhydrophilic layer. After 65 s, the droplets on the surface of the hydrophobic layer disappeared, but they left a wet mark that was slightly larger than the initial droplet. When the droplets of different volumes (25, 50, or 100 μL) were added to the hydrophobic layer, their spreading diameter remained unchanged after 5 s; the largest spreading diameters were 0.36, 0.5, and 0.629 cm, respectively (Fig. 4c). When the droplets were added on the superhydrophilic layer, the initial spreading diameter of the droplet with the same volume on the superhydrophilic layer was larger than that on the hydrophobic layer. The spreading diameters of 25, 50, and 100 μL droplets on the hydrophilic layer were 0.84, 1.45, and 1.77 cm, respectively (Fig. 4d), and the droplet spreading diameter significantly increased with larger droplet volumes. Therefore, the drug liquid can be transported directly from the hydrophobic to the superhydrophilic layer and can extend to a certain area to be administered to the wound (Fig. 4e).

The underlying mechanism of this process was analyzed (Fig. 4f). Combining the above discussion, the directional transport of water can be explained by the following theoretical quasi-static model. In the first stage, a droplet was added to the hydrophobic layer and initially retained a Wenzel–Cassie state. In the second stage, the drug droplet permeated downward owing to the downward capillary force and gravity. When the drug droplet arrived at the interface of the hydrophobic/superhydrophilic layers, the generated capillary pressure difference (ΔP) was calculated using Eq. 7, ΔP (P_{L2}–P_{L1}) <0; thus, ΔP plays a crucial role in the driving force that transports the drug droplet directly from the hydrophobic layer into the superhydrophilic layer. Once the drug droplet enters the superhydrophilic layer, it rapidly diffuses.

3.4 Antibacterial properties and bacterial antiadhesion of the Janus composite membrane

Bacterial infections can delay wound healing. Therefore, it is necessary to use wound plaster that have antibacterial properties. The antibacterial effect of the Janus composite dressing was derived from chitosan and triangular silver nanoprisms. A PVA/CS@TPU membrane without silver was compared with the Janus composite membrane containing chitosan and silver. A large number of bacteria were observed in the control group (Fig. S4). Conversely, a small number of bacteria were observed in the PVA/CS@TPU membrane group. Almost no bacteria were detected on the Petri dish in the Janus composite membrane (PVA/CS/Ag@TPU) group. The antibacterial rates of *E. coli* and *S. aureus* in the PVA/CS@TPU membrane group were 95.87% and 97.91%, respectively (Fig. 5a). The antibacterial rates of the Janus composite membrane (PVA/CS/Ag@TPU) were further enhanced to 99.9% and 99.9%, respectively. Live/dead bacteria were observed via fluorescence-staining microscopy where green and red fluorescence represented the live and dead bacteria, respectively. In the control group, the samples mainly comprised live bacteria. In the Janus composite membrane (PVA/CS/Ag@TPU) group, there were a large number of dead bacteria and a small number

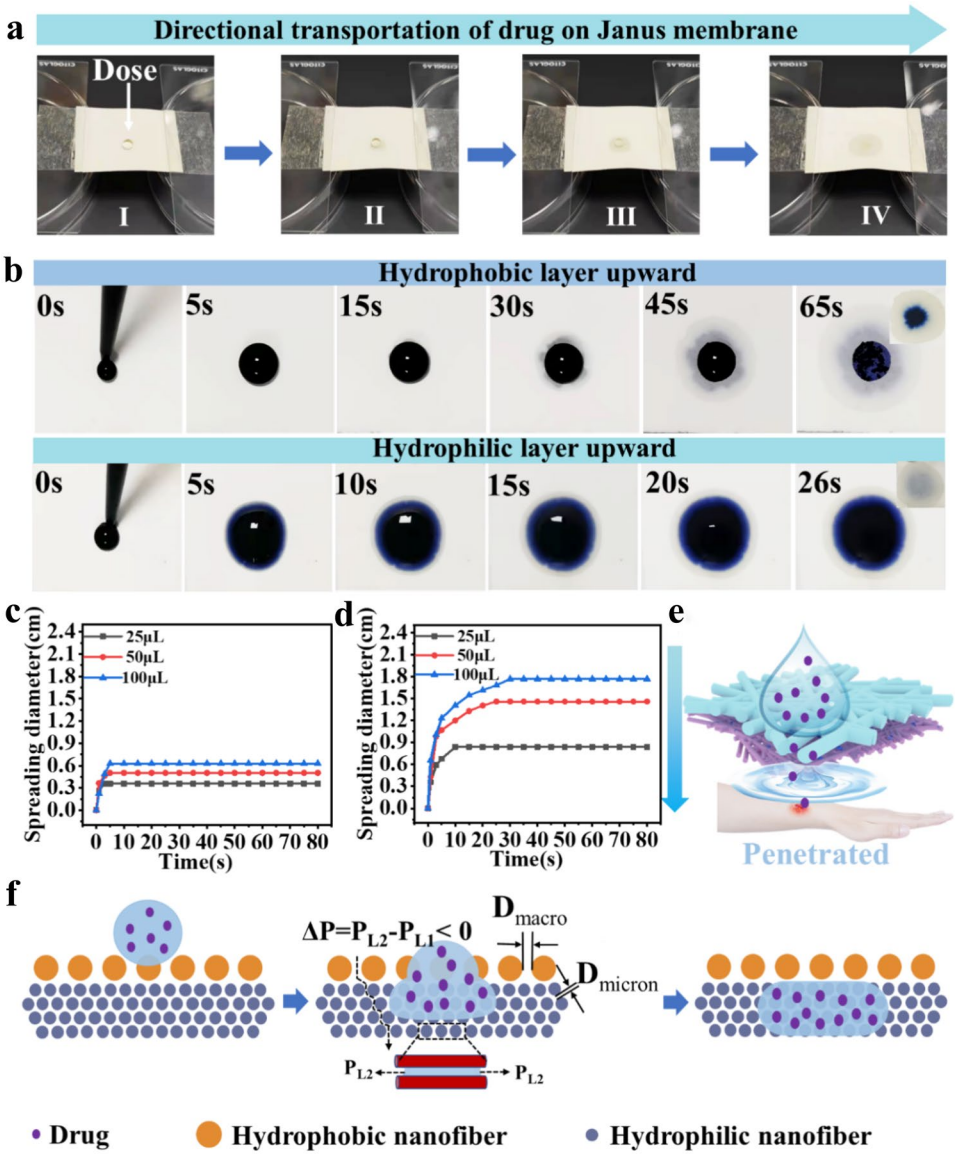

Fig. 4 Photographs of **a** unidirectional transportation behavior on the Janus composite membrane (hydrophobic layer upward). **b** The water transportation behavior on the Janus membrane after adding a water droplet (50 μL) on the hydrophobic and superhydrophilic layers; relationship between a water droplet's spreading diameter with time when droplets of different volumes were dropped on the **c** hydrophobic layer and **d** superhydrophilic layer of the Janus composite membrane. **e** Schematic diagram of the directional transportation of drug liquid in the Janus composite membrane. **f** Illustration of the directional transport mechanism of the drug liquid (ΔP: capillary pressure difference)

of live bacteria. In the fluorescence images of *E. coli* and *S. aureus* in the Janus composite membrane group (PVA/CS/Ag@TPU), all bacteria were dead (Fig. 5b). The above antibacterial comparison experiments revealed that chitosan and silver nanoprisms introduced by the Janus composite membrane exhibit good antibacterial activity against *E. coli* and *S. aureus*, and the silver nanoprisms further improved the antibacterial rate of the membrane.

In addition to its antibacterial properties, the wound plaster needs to prevent bacteria from adhering because even a small number of bacteria can cause wound inflammation and bacterial infection. The bacterial antiadhesion ability of the PVA membrane and superhydrophilic layer of the PVA/CS/Ag membrane was consequently assessed. The bacterial counts of *E. coli* and *S. aureus* on the plates in the PVA membrane and PVA/CS/Ag membrane groups were lower than those in the control group (tenfold dilution of 10^7 CFU/mL bacterial solution three times), consistent with the fluorescence microscopy results (Fig. 5c, d). The bacterial antiadhesion property of the PVA/CS/Ag membrane was better than that of the PVA membrane, which was attributed to the antibacterial effects of PVA/CS/Ag. The excellent bacterial antiadhesion ability of the PVA/CS/Ag membrane is related to oil adhesion and underwater hydrophobicity. A certain adhesion force (0.00589 mN) was observed on the surface of the PVA membrane, and the underwater oil contact angle was 136.7° (Fig. 5e). Furthermore, the adhesion force of the PVA/CS/Ag membrane to oily substances was almost zero, and the underwater oil contact angle was 143.2° (Fig. 5f). The bacterial antiadhesion mechanism of the Janus composite membrane was further analyzed (Fig. 5g). When the PVA/CS/Ag superhydrophilic

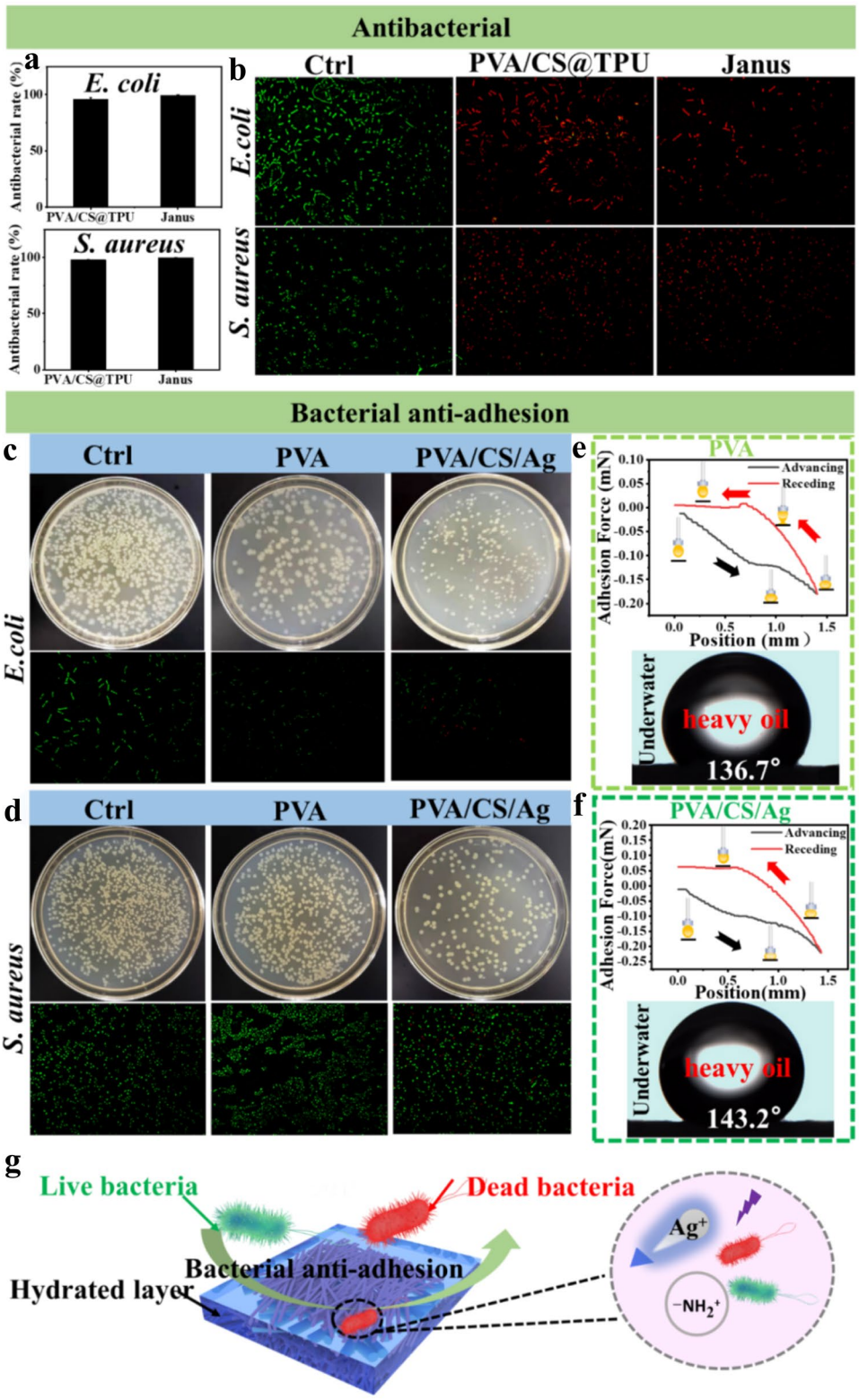

Fig. 5 **a** Antibacterial rate of different samples against *E. coli* and *S. aureus*. **b** Fluorescence microscopy images after the antibacterial test of different samples against *E. coli* and *S. aureus*. Bacterial colonies after the bacterial antiadhesion test of different samples against **c** *E. coli* and **d** *S. aureus*. Adhesive force curve and underwater oil contact angle of the **e** PVA and **f** PVA/CS/Ag membranes. **g** Schematic diagram of the bacterial antiadhesion mechanism of the Janus membrane

layer absorbs water from blood or comes into contact with water in the blood through PVA and water molecules and forms a hydration layer, the hydration layer can resist lipophilic substances and block bacterial adhesion because the bacterial cell walls are lipophilic. The bacterial antiadhesion effect of the hydration layer has also been reported in the previous works [57, 58, 66, 67]. In addition, the synergistic antibacterial action of chitosan and silver can reduce the

total amount of bacteria. Chitosan has a positively charged amino group, which can inhibit bacterial activity. Triangular silver nanoprisms release Ag^+ to interfere with cellular respiration enzymes, preventing the reproduction of bacteria and reducing bacterial adhesion to the membrane surface.

3.5 Animal wound-healing experiment

Animal experiments were conducted on mice to replicate wound healing in the human body. A circular wound with a 7-mm diameter was made on the back of each mouse. The wounds were treated with different dressing samples to promote wound healing (Fig. 6a). Subsequently, wound healing in each group was observed over a period of 10 days. The wound area decreased gradually in the order of medical gauze < PVA membrane < Janus composite membrane < Janus composite membrane + liquid drug (Fig. 6b). The wound-healing rate was the fastest in the first 4 days (Fig. 6). The percentage of the wound area in the mice treated with medical gauze, PVA membrane, Janus composite membrane, and Janus composite membrane plus liquid drug were 55.04%, 50.48%, 41.22%, and 24.67%, respectively. After 4 days, the wound-healing rate slowed down. Until the 10^{th} day, the wound-healing rates of the mice treated with the Janus composite membrane plus liquid drug were almost 100%. On the 10^{th} day, the percentage of the wound area in mice treated with medical gauze, PVA membrane, Janus composite membrane, and Janus composite membrane plus liquid drug were 21.39%, 16.68%, 12.35%, and 2.39%, respectively. The weight of the mice treated with the medical gauze and PVA membrane exhibited a slightly decreasing trend, indicating that the wound affected their health. Conversely, the weight of the mice treated with the Janus composite membrane or Janus composite membrane plus liquid drug exhibited an increasing trend, indicating wound healing. On the 10^{th} day, the percentage of body weight gain of the mice treated with medical gauze, PVA membrane, Janus

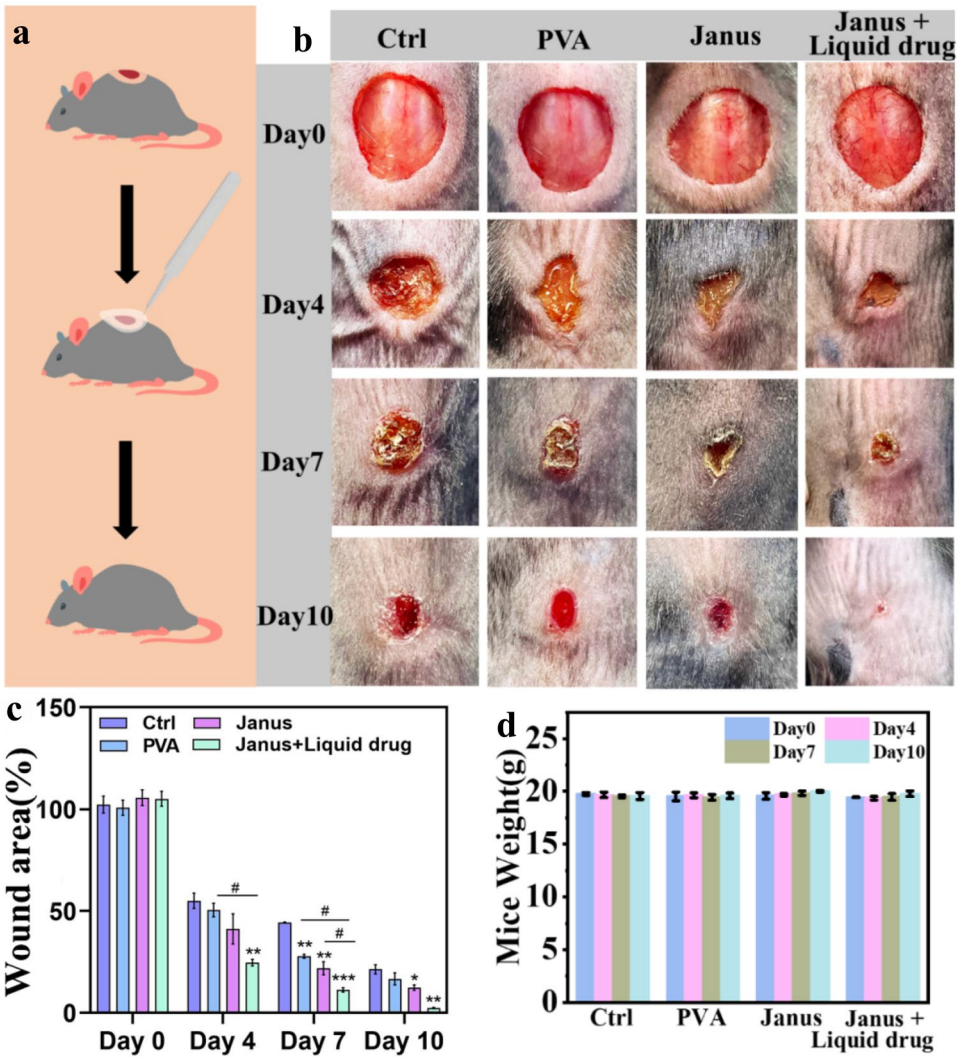

Fig. 6 **a** Schematic diagram of the animal experiment process. **b** Photographs of wounds after treatment with different samples. **c** The wound area and **d** weight of mice were measured at different times (days). Data are represented by mean ± SD of three repeats, $*p < 0.05$, $**p < 0.01$, $***p < 0.001$ as compared with the control, $^{\#}p < 0.05$ as compared with designated group

composite membrane, and Janus composite membrane plus liquid drug were − 0.98%, 0.29%, 2.22%, and 1.68%, respectively (Fig. 6d). Overall, the therapeutic effect of the PVA membrane was better than that of medical gauze, which proves the superiority of the electrospun nanofiber structure in promoting wound healing. The treatment effect of the Janus composite membrane was greater than that of the PVA membrane, which confirms the coagulation and antibacterial effects of chitosan and triangular silver nanoprisms on promoting wound healing. The effect of the Janus composite membrane plus liquid drug therapy was greater than that of the Janus composite membrane alone, which proved that the Janus membrane allows the directional transport of the liquid drug, which promotes wound healing.

The H&E-stained sections of the regener ated tissues revealed that the degree of wound healing in each group of mice increased with increasing healing time, while the wound-healing degree of the mice treated with the Janus composite membrane plus liquid drug was optimum (Fig. 7a). On day 4, new hair follicles appeared in the subcutaneous tissue of the mice treated with the Janus composite membrane plus liquid drug. Therefore, the Janus composite membrane plus liquid drug treatment formed a good wound bed environment for the mice. On day 7, intact tissue layers appeared in some healed areas. On day 10, the subcutaneous tissue of mice in this group was intact, and the thickness of the epidermis and granulation tissues was lower than that of the other groups (Fig. 7b, c). Conversely, the other groups required a longer time to complete wound

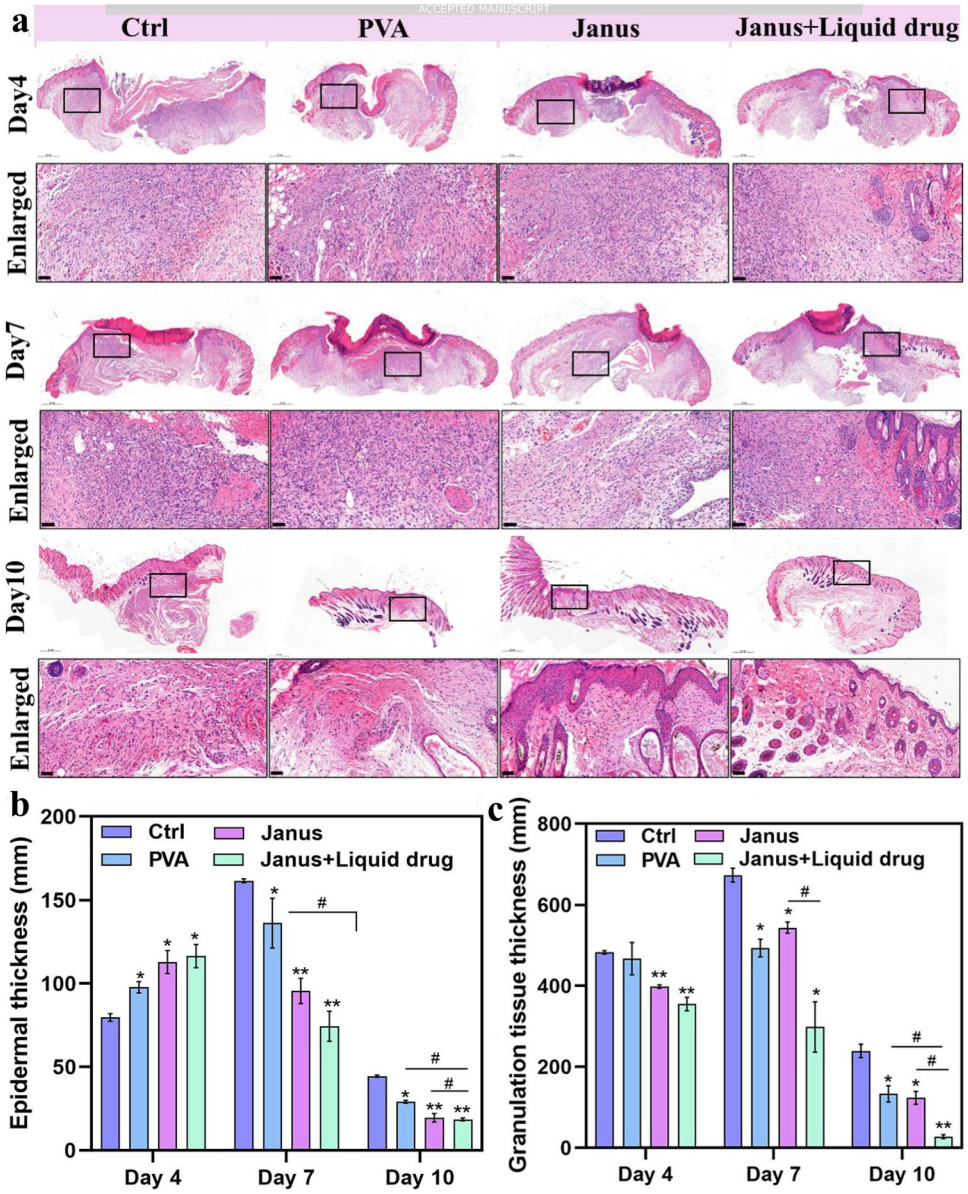

Fig. 7 **a** H&E-stained section of regenerated skin tissue treated with the different materials at different timepoints (days) (Scale bar = 50 μm); **b** epidermal and **c** granulation tissue thicknesses after treatment with the different materials at different times (days). Data are represented by mean ± SD of three repeats, $*p < 0.05$, $**p < 0.01$ as compared with the control, $^{\#}p < 0.05$ as compared with designated group

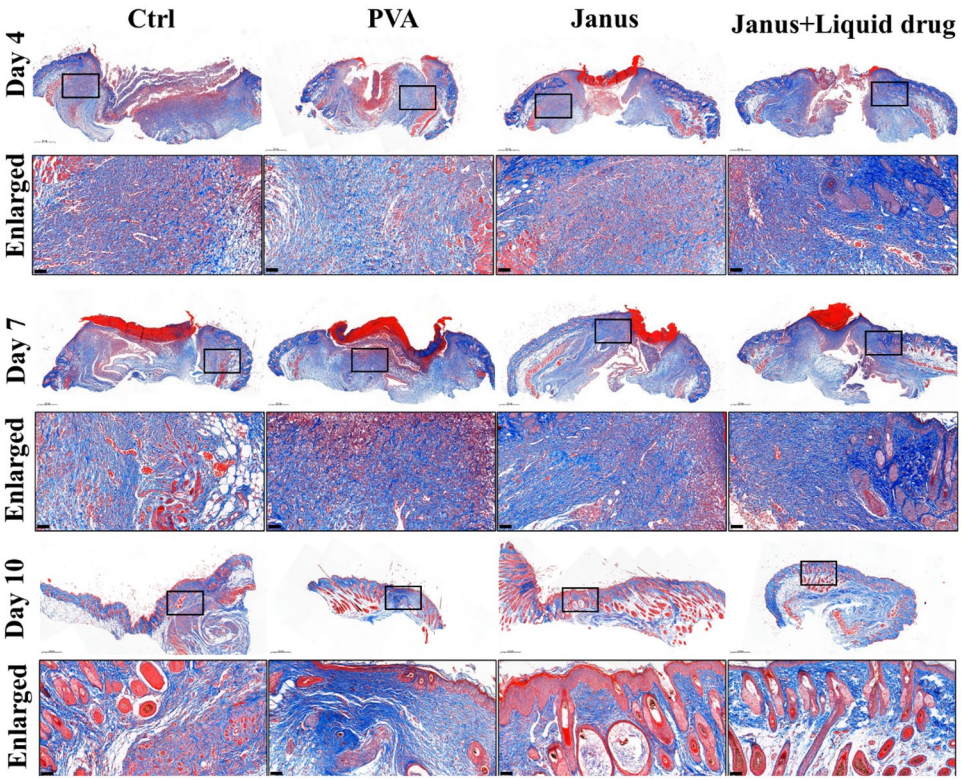

Fig. 8 Masson-stained sections of regenerated skin tissue treated with different samples for different times (days) (Scale bar = 50 μm)

remodeling. Hypertrophy of the epidermis and granulation tissue creates scar formation, and the scar size of the mice treated with the Janus composite membrane plus liquid drug was the smallest.

The Masson-stained sections of the regenerated tissues were used to analyze the changes in collagen content during wound healing. Masson staining revealed that the collagen content in each group gradually increased with

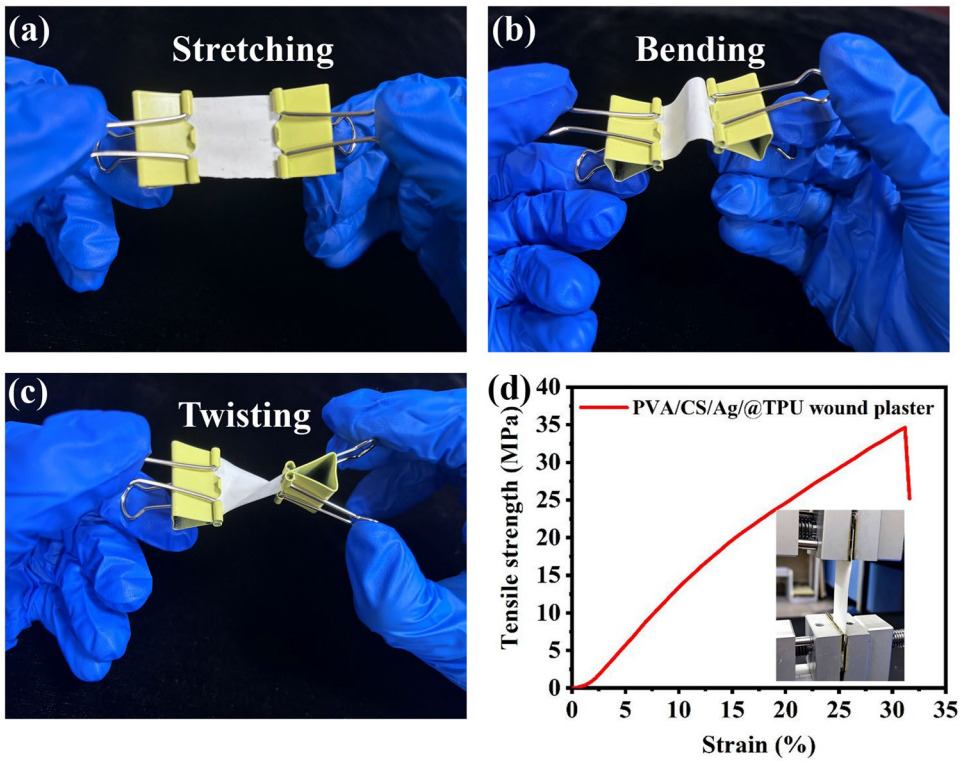

Fig. 9 Mechanical properties of PVA/CS/Ag/@TPU wound plaster **a** Stretching; **b** Bending; **c** Twisting; **d** Strain-tensile strength curves

treatment time (Fig. 8). On day 10, the collagen fibers of the mice treated with the Janus composite membrane plus liquid drug were aligned. Furthermore, this group exhibited higher collagen content than the other groups (Fig. S5), indicating a higher quality of regenerated tissue. These results demonstrate that the coagulation, antibacterial, bacterial antiadhesion, and liquid drug directional transportation properties of the Janus composite membrane promotes rapid wound healing.

3.6 Mechanical performance of wound plaster

As a wound plaster, it usually needs to have good mechanical properties in many aspects in order to facilitate its use, and it is required to fit with the skin wound to reflect its comfort, for this reason, its basic physical mechanical properties are investigated. As shown in Fig. 9, PVA/CS/Ag/@TPU wound plaster displays not only outstanding stretching, bending, twisting physical performance, but also superior mechanical properties with tensile strength of 34.6 MPa and elongation at break of 31.1%, which can be considered close to the human skin, with a tensile strength of 21.6 ± 8.4 MPa and failure strain of $54 \pm 17\%$ [48].

4 Conclusions

A novel fibrous Janus membrane wound plaster (PVA/CS/Ag@TPU) with superhydrophilic/hydrophobic wettability was produced using electrospinning technology, which realized the functional integrations of hemostasis, antibacterial synergistic antiadhesion, and directional transportation of liquid drugs to promote wound healing. The efficient hemostasis of this membrane was attributed to the rapid water absorption by the hydrophilic layer from the blood, capillary pressure difference ($\Delta p > 0$) that prevented the extravasation of blood, and coagulation promoted by chitosan. Thus, wound healing can be achieved through the effective combination of antibacterial synergistic antiadhesion and directional transportation of liquid drugs. Chitosan and silver imparted the Janus membrane with high antibacterial (99.9% against *E. coli* and 99.9% against *S. aureus*) and bacterial antiadhesion properties because of low underwater oil adhesion, hydration layer formation, and excellent antibacterial ability. The excellent directional transportation of the liquid drug was attributed to the favorable Δp from the hydrophobic to the superhydrophilic layer. After 10 days, the regenerated skin tissue of mice treated with the Janus composite membrane plus liquid drug exhibited smaller scar size and more suitable lamellar structure compared with the tissues in the other groups. The small scar size and intact tissue layer structure of the Janus composite membrane and liquid drug–assisted regenerated skin tissue effectively promoted collagen growth. The wound-healing rate of the mice reached 97.61% in this group. Therefore, the Janus composite membrane exhibits good clinical application potential and provides design inspiration for the development of next-generation wound plaster.

Supplementary Information The online version contains supplementary material available at https://doi.org/10.1007/s42114-023-00764-8.

Author contributions Jing Lin contributed to the design of experiments, the writing, and revision of papers. Zhen Yao, Jin Lin, and Minmin Xiong contributed to the experimental perform and analysis. Fei Hu, Xinchuan Wei, and Songyin Huang contributed to the revision of the paper and project funding. All authors reviewed the manuscript.

Funding This work is financially supported by the National Natural Science Foundation of China (No.22078077), Science and Technology Planning Project of Qingyuan (Nos.2019DZX023, 2020DZX015), the Natural Science Foundation of Guangdong Province grant (2021A1515010283), and the Foundation of Guangzhou Science and Technology Bureau (202201020302).

Data availability Data will be made available on request.

Declarations

Competing interests The authors declare no competing interests.

References

1. Zhou FF, Yang Y, Zhang WJ, Liu SY, Shaikh AB, Yang L, Lai YX, Ouyang HW, Zhu WM (2022) Bioinspired, injectable, tissue-adhesive and antibacterial hydrogel for multiple tissue regeneration by minimally invasive therapy. Appl Mater Today 26:101290. https://doi.org/10.1016/j.apmt.2021.101290
2. Hartgerink JD (2006) New material stops bleeding in a hurry. Nature Nanotech 1:166–167. https://doi.org/10.1038/nnano.2006.148
3. Curry NS, Davenport RA, Hunt BJ, Stanworth SJ (2012) Transfusion strategies for traumatic coagulopathy. Blood Rev 26:223–232. https://doi.org/10.1016/j.blre.2012.06.004
4. Bakadia BM, Zhong A, Li X, Boni BOO, Ahmed AAQ, Souho T, Zheng R, Shi Z, Shi D, Lamboni L, Yang G (2022) Biodegradable and injectable poly(vinyl alcohol) microspheres in silk sericin-based hydrogel for the controlled release of antimicrobials: Application to deep full-thickness burn wound healing. Adv Compos Hybrid Mater 5(4):2847–2872. https://doi.org/10.1007/s42114-022-00467-6

5. Boni BO, Lamboni L, Mao L, Bakadia BM, Shi Z, Yang G (2022) In vivo performance of microstructured bacterial cellulose-silk sericin wound dressing: Effects on fibrosis and scar formation. Eng Sci. https://doi.org/10.30919/es8d700
6. Boni BO, Lamboni L, Bakadia BM, Hussein SA, Yang G (2020) Combining silk sericin and surface micropatterns in bacterial cellulose dressings to control fibrosis and enhance wound healing. Eng Sci. https://doi.org/10.30919/es8d906
7. Malik A, Rehman FU, Shah KU, Naz SS, Qaisar S (2021) Hemostatic strategies for uncontrolled bleeding: A comprehensive update. J Biomed Mater Res B Appl Biomater 109:1465–1477. https://doi.org/10.1002/jbm.b.34806
8. Rahmany MB, Hantgan RR, Van Dyke M (2013) A mechanistic investigation of the effect of keratin-based hemostatic agents on coagulation. Biomaterials 34:2492–2500. https://doi.org/10.1016/j.biomaterials.2012.12.008
9. Ding YF, Huang QX, Quan XP, Cheng Q, Li SK, Zhao YH, Mok GSP, Wang RB (2022) Supramolecularly functionalized platelets for rapid control of hemorrhage. Acta Biomater 149:248–257. https://doi.org/10.1016/j.actbio.2022.07.007
10. Kauvar DS, Lefering R, Wade CE (2006) Impact of hemorrhage on trauma outcome: an overview of epidemiology, clinical presentations, and therapeutic considerations. J Trauma 60:S3–S9. https://doi.org/10.1097/01.ta.0000199961.02677.19
11. Mulholland EK, Adegbola RA (2005) Bacterial infections - A major cause of death among children in Africa. New Engl J Med 352:75–77. https://doi.org/10.1056/nejme048306
12. Ciofu O, Moser C, Jensen PO, Hoiby N (2022) Tolerance and resistance of microbial biofilms. Nat Rev Microbiol. https://doi.org/10.1038/s41579-022-00682-4
13. Ahmed W, Zhai Z, Gao C (2019) Adaptive antibacterial biomaterial surfaces and their applications. Materials Today Bio 2:100017. https://doi.org/10.1016/j.mtbio.2019.100017
14. Fang J, Wan Y, Sun Y, Sun XL, Qi ML, Cheng S, Li CY, Zhou YM, Xu L, Dong B, Wang L (2022) Near-infrared-activated nanohybrid coating with black phosphorus/zinc oxide for efficient biofilm eradication against implant-associated infections. Chem Eng J 435:134935. https://doi.org/10.1016/j.cej.2022.134935
15. Kharaziha M, Baidya A, Annabi N (2021) Rational design of immunomodulatory hydrogels for chronic wound healing. Adv Mater 33:2100176. https://doi.org/10.1002/adma.202100176
16. Li WL, Thian ES, Wang M, Wang ZY, Ren L (2021) Surface design for antibacterial materials: From fundamentals to advanced strategies. Adv Sci 8:2100368. https://doi.org/10.1002/advs.202100368
17. Behrens AM, Sikorski MJ, Kofinas P (2014) Hemostatic strategies for traumatic and surgical bleeding. J Biomed Mater Res A 102:4182–4194. https://doi.org/10.1002/jbm.a.35052
18. Vaiana CA, Leonard MK, Drummy LF, Singh KM, Bubulya A, Vaia RA, Naik RR, Kadakia MP (2011) Epidermal growth factor: layered silicate nanocomposites for tissue regeneration. Biomacromolecules 12:3139–3146. https://doi.org/10.1021/bm200616v
19. Pourshahrestani S, Zeimaran E, Kadri NA, Mutlu N, Boccaccini AR (2020) Boccaccini, and Polymeric hydrogel systems as emerging biomaterial platforms to enable hemostasis and wound healing. Adv Healthcare Mater 9:2000905. https://doi.org/10.1002/adhm.202000905
20. Wang XX, Liu Q, Sui JX, Ramakrishna S, Yu M, Zhou Y, Jiang XY, Long YZ (2019) Recent advances in hemostasis at the nanoscale. Adv Healthcare Mater 8:1900823. https://doi.org/10.1002/adhm.201900823
21. Teng L, Shao ZW, Bai Q, Zhang XL, He YS, Lu JY, Zou DR, Feng CL, Dong CM (2021) Biomimetic glycopolypeptide hydrogels with tunable adhesion and microporous structure for fast hemostasis and highly efficient wound healing. Adv Funct Mater 31:2105628. https://doi.org/10.1002/adfm.202105628
22. Peng X, Xu X, Deng YR, Xie X, Xu LM, Xu XY, Yuan WH, Yang BG, Yang XF, Xia XF, Duan L, Bian LM (2021) Ultrafast self-gelling and wet adhesive powder for acute hemostasis and wound healing. Adv Funct Mater 31:2102583. https://doi.org/10.1002/adfm.202102583
23. Cui CY, Fan CC, Wu YH, Xiao M, Wu TL, Zhang DF, Chen XY, Liu B, Xu ZY, Qu B, Liu WG (2019) Water-triggered hyperbranched polymer universal adhesives: From strong underwater adhesion to rapid sealing hemostasis. Adv Mater 31:1905761. https://doi.org/10.1002/adma.201905761
24. Liu CY, Liu X, Liu CY, Wang N, Chen HL, Yao WH, Sun GZ, Song QL, Qiao WHA (2019) highly efficient, in situ wet-adhesive dextran derivative sponge for rapid hemostasis. Biomaterials 205:23–37. https://doi.org/10.1016/j.biomaterials.2019.03.016
25. Zhang XX, Chen GP, Cai LJ, Wang YT, Sun LY, Zhao YJ (2021) Bioinspired pagoda-like microneedle patches with strong fixation and hemostasis capabilities. Chem Eng J 414:128905. https://doi.org/10.1016/j.cej.2021.128905
26. Shi ZH, Lan GQ, Hu EL, Lu F, Qian P, Liu JW, Dai FY, Xie RQ (2022) Targeted delivery of hemostats to complex bleeding wounds with magnetic guidance for instant hemostasis. Chem Eng J 427:130916. https://doi.org/10.1016/j.cej.2021.130916
27. Zhang J, Zhao YT, Hu PY, Liu JJ, Liu XF, Hu MZ, Cui ZM, Wang N, Niu ZY, Xiang HF, Long YZ (2020) Laparoscopic electrospinning for in situ hemostasis in minimally invasive operation. Chem Eng J 395:125089. https://doi.org/10.1016/j.cej.2020.125089
28. Yan LL, Yang XB, Zhang YQ, Wu YD, Cheng ZJ, Darling SB, Shao L (2021) Porous Janus materials with unique asymmetries and functionality. Mater Today 51:626–647. https://doi.org/10.1016/j.mattod.2021.07.001
29. Luo Z, Jiang L, Xu CF, Kai D, Fan XS, You ML, Hui CM, Wu CS, Wu YL, Li ZB (2021) Engineered Janus amphipathic polymeric fiber films with unidirectional drainage and anti-adhesion abilities to accelerate wound healing. Chem Eng J 421:127725. https://doi.org/10.1016/j.cej.2020.127725
30. Bao F, Pei G, Wu ZC, Zhuang H, Zhang ZWB, Huan ZG, Wu CT, Chang J (2020) Bioactive self-pumping composite wound dressings with micropore array modified Janus membrane for enhanced diabetic wound healing. Adv Funct Mater 30:2005422. https://doi.org/10.1002/adfm.202005422
31. Xu B, Li A, Wang R, Zhang J, Ding YL, Pan D, Shen ZJ (2021) Elastic Janus film for wound dressings: Unidirectional biofluid transport and effectively promoting wound healing. Adv Funct Mater 31:2105265. https://doi.org/10.1002/adfm.202105265
32. Si Y, Li J, Cui B, Tang D, Yang L, Murugadoss V, Maganti S, Huang M, Guo Z (2022) Janus phenol–formaldehyde resin and periodic mesoporous organic silica nanoadsorbent for the removal of heavy metal ions and organic dyes from polluted water. Adv Compos Hybrid Mater 5(2):1180–1195. https://doi.org/10.1007/s42114-022-00446-x
33. Guan X, Zhang Q, Dong C, Zhang R, Peng M, Liu G, Lei M, Lu P (2022) A first-principles study of janus monolayer mxy (m = mo, w; x, y = s, se, te)/sio2 van der waals heterojunctions for integrated optical fibers. Adv Compos Hybrid Mater 5(4):3232–3244. https://doi.org/10.1007/s42114-022-00557-5
34. Zhu T, Wu JR, Zhao N, Cai C, Qian ZC, Si FF, Luo H, Guo J, Lai X, Shao LQ, Xu J (2018) Superhydrophobic/superhydrophilic Janus fabrics reducing blood loss. Adv Healthcare Mater 7:1701086. https://doi.org/10.1002/adhm.201701086
35. Zhao X, Wu H, Guo BL, Dong RN, Qiu YS, Ma PX (2017) Antibacterial anti-oxidant electroactive injectable hydrogel as self-healing wound dressing with hemostasis and adhesiveness for cutaneous wound healing. Biomaterials 122:34–47. https://doi.org/10.1016/j.biomaterials.2017.01.011
36. Ming ZZ, Han L, Bao MY, Zhu HH, Qiang SJ, Xue SB, Liu WW (2021) Living bacterial hydrogels for accelerated infected

wound healing. Adv Sci 8:2102545. https://doi.org/10.1002/advs.202102545
37. Li MN, Li N, Qiu WW, Wang Q, Jia J, Wang XL, Yu JY, Li XR, Li FX, Wu DQ (2022) Phenylalanine-based poly(ester urea) s composite films with nitric oxide-releasing capability for antibiofilm and infected wound healing applications. J Colloid Interf Sci 607:1849–1863. https://doi.org/10.1016/j.jcis.2021.10.016
38. Liang YQ, Li ZL, Huang Y, Yu R, Guo BL (2021) Dual-dynamic-bond cross-Linked antibacterial adhesive hydrogel sealants with on-demand removability for post-wound-closure and infected wound healing. ACS Nano 15:7078–7093. https://doi.org/10.1021/acsnano.1c00204
39. Liu YN, Li F, Guo ZR, Xiao YQ, Zhang YL, Sun XY, Zhe TT, Cao YY, Wang L, Lu QY, Wang JH (2020) Silver nanoparticle-embedded hydrogel as a photothermal platform for combating bacterial infections. Chem Eng J 382:122990. https://doi.org/10.1016/j.cej.2019.122990
40. Yue YP, Gong XB, Jiao WL, Li Y, Yin X, Si Y, Yu JY, Ding B (2021) in situ electrospinning of thymol-loaded polyurethane fibrous membranes for waterproof, breathable, and antibacterial wound dressing application. J Colloid Interf Sci 592:310–318. https://doi.org/10.1016/j.jcis.2021.02.048
41. Khan AUR, Huang K, Zhao JZ, Zhu TH, Morsi Y, Aldalbahi A, El-Newehy M, Yan XY, Mo XM (2021) Exploration of the antibacterial and wound healing potential of a PLGA/silk fibroin-based electrospun membrane loaded with zinc oxide nanoparticles. J Mater Chem B 9:1452–1465. https://doi.org/10.1039/d0tb02822c
42. Sun GM, Shen YI, Harmon JW (2018) Engineering pro-regenerative hydrogels for scarless wound healing. Adv Healthcare Mater 7:1800016. https://doi.org/10.1002/adhm.201800016
43. Yu R, Zhang HL, Guo BL (2022) Conductive biomaterials as bioactive wound dressing for wound healing and skin tissue engineering. Nano-Micro Lett 14:1. https://doi.org/10.1007/s40820-021-00751-y
44. Chen GP, Yu YR, Wu XW, Wang GF, Ren JN, Zhao YJ (2018) Bioinspired multifunctional hybrid hydrogel promotes wound healing. Adv Funct Mater 28:1801386. https://doi.org/10.1002/adfm.201801386
45. Wang M, Wang CG, Chen M, Xi YW, Cheng W, Mao C, Xu TZ, Zhang XX, Lin C, Gao WY, Guo Y, Lei B (2019) Efficient angiogenesis-based diabetic wound healing/skin reconstruction through bioactive antibacterial adhesive ultraviolet shielding nanodressing with exosome release. ACS Nano 13:10279–10293. https://doi.org/10.1021/acsnano.9b03656
46. Gao C, Zhang LY, Wang J, Jin M, Tang QQ, Chen ZR, Cheng Y, Yang RH, Zhao G (2021) Electrospun nanofibers promote wound healing: theories, techniques, and perspectives. J Mater Chem B 9:3106–3130. https://doi.org/10.1039/d1tb00067e
47. Ghosal K, Agatemor C, Spitalsky Z, Thomas S, Kny E (2019) Electrospinning tissue engineering and wound dressing scaffolds from polymer-titanium dioxide nanocomposites. Chem Eng J 358:1262–1278. https://doi.org/10.1016/j.cej.2018.10.117
48. Dias JR, Granja PL, Bártolo PJ (2016) Advances in electrospun skin substitutes. Prog Mater Sci 84:314–334. https://doi.org/10.1016/j.pmatsci.2016.09.006
49. Wang T, Wusigale, Kuttappan D, Amalaradjou MA, Luo Y, Luo Y (2021) Polydopamine-coated chitosan hydrogel beads for synthesis and immobilization of silver nanoparticles to simultaneously enhance antimicrobial activity and adsorption kinetics. Adv Compos Hybrid Mater 4(3):696–706. https://doi.org/10.1007/s42114-021-00305-1
50. Xiao L, Xu W, Huang L, Liu J, Yang G (2022) Nanocomposite pastes of gelatin and cyclodextrin-grafted chitosan nanoparticles as potential postoperative tumor therapy. Adv Compos Hybrid Mater 6(1). https://doi.org/10.1007/s42114-022-00575-3
51. Ran F, Li C, Hao Z, Zhang X, Dai L, Si C, Shen Z, Qiu Z, Wang J (2022) Combined bactericidal process of lignin and silver in a hybrid nanoparticle on e. Coli Adv Compos Hybrid Mater 5(3):1841–1851. https://doi.org/10.1007/s42114-022-00460-z
52. Huang K, Liu J, Lin S, Wu Y, Chen E, He Z, Lei M (2021) Flexible silver nanowire dry electrodes for long-term electrocardiographic monitoring. Adv Compos Hybrid Mater 5(1):220–228. https://doi.org/10.1007/s42114-021-00322-0
53. Jin RC, Cao YW, Mirkin CA, Kelly KL, Schatz GC, Zheng JG (2001) Photoinduced conversion of silver nanospheres to nanoprisms. Science 294:1901–1903. https://doi.org/10.1126/science.1066541
54. Dong XY, Ji XH, Jing J, Li MY, Li J, Yang WS (2010) Synthesis of triangular silver nanoprisms by stepwise reduction of sodium borohydride and trisodium citrate. J Phys Chem C 114:2070–2074. https://doi.org/10.1021/jp909964k
55. Lin J, Cai XF, Liu ZL, Liu N, Xie M, Zhou BP, Wang HQ, Guo ZH (2020) Anti-liquid-interfering and bacterially antiadhesive strategy for highly stretchable and ultrasensitive strain sensors based on cassie-baxter wetting state. Adv Funct Mater 30:2000398. https://doi.org/10.1002/adfm.202000398
56. Lin J, Hu JT, Wang W, Liu KL, Zhou CL, Liu ZL, Kong SF, Lin SD, Deng YC, Guo ZH (2021) Thermo and light-responsive strategies of smart titanium-containing composite material surface for enhancing bacterially anti-adhesive property. Chem Eng J 407:125783. https://doi.org/10.1016/j.cej.2020.125783
57. Lin J, Wang YF, Wei XC, Kong SF, Liu ZL, Liu JJ, Zhang FM, Lin SD, Ji B, Zhou ZZ, Guo ZH (2020) Controllable antibacterial and bacterially anti-adhesive surface fabricated by a bio-inspired beetle-like macromolecule. Int J Biol Macromol 157:553–560. https://doi.org/10.1016/j.ijbiomac.2020.04.207
58. Lin J, Chen XY, Chen CY, Hu JT, Zhou CL, Cai XF, Wang W, Zheng C, Zhang PP, Cheng J, Guo ZH, Liu H (2018) Durably antibacterial and bacterially antiadhesive cotton fabrics coated by cationic fluorinated polymers. Acs Appl Mater Inter 10:6124–6136. https://doi.org/10.1021/acsami.7b16235
59. Chen Y, Lin J, Mersal GAM, Zuo JL, Li JL, Wang QY, Feng YH, Liu JW, Liu ZL, Wang B, Xu BB, Guo ZH (2022) Several birds with one -stone" strategy of pH/thermoresponsive flame-retardant/photothermal bactericidal oil-absorbing material for recovering complex spilled oil. J Mater Sci Technol 128:82–97. https://doi.org/10.1016/j.jmst.2022.05.002
60. Hu JT, Gui LS, Zhu MN, Liu KL, Chen Y, Wang XP, Lin J (2022) Smart Janus membrane for on-demand separation of oil, bacteria, dye, and metal ions from complex wastewater. Chem Eng Sci 253:117586. https://doi.org/10.1016/j.ces.2022.117586
61. Wang YF, Liu ZL, Wei XC, Liu KL, Wang JH, Hu JT, Lin J (2021) An integrated strategy for achieving oil-in-water separation, removal, and anti-oil/dye/bacteria-fouling. Chem Eng J 413:127493. https://doi.org/10.1016/j.cej.2020.127493
62. Hou CX, Yang WY, Kimura H, Xie XB, Zhang XY, Sun XQ, Yu ZP, Yang XY, Zhang YP, Wang B, Xu BB, Sridhar D, Algadi H, Guo ZH, Du W (2023) Boosted lithium storage performance by local build-in electric field derived by oxygen vacancies in 3D holey N-doped carbon structure decorated with molybdenum dioxide. J Mater Sci Technol 142:185–195. https://doi.org/10.1016/j.jmst.2022.10.007
63. Li FS, Li QY, Kimura H, Xie XB, Zhang XY, Wu NN, Sun XQ, Xu BB, Algadi H, Pashameah RA, Alanazi AK, Alzahrani E, Li HD, Du W, Guo ZH, Hou CX (2023) Morphology controllable urchin-shaped bimetallic nickel-cobalt oxide/carbon composites with enhanced electromagnetic wave absorption performance. J Mater Sci Technol 148:250–259. https://doi.org/10.1016/j.jmst.2022.12.003
64. Mu Q, Liu RL, Kimura H, Li JC, Jiang HY, Zhang XY, Yu ZP, Sun XQ, Algadi H, Guo ZH, Du W, Hou CX (2023) Supramolecular

self-assembly synthesis of hemoglobin-like amorphous CoP@N, P-doped carbon composites enable ultralong stable cycling under high-current density for Lithium-ion battery anodes. Adv Compos Hybrid Mater 6:23. https://doi.org/10.1007/s42114-022-00607-y

65. Hou Y, Carrim N, Wang Y, Gallant RC, Marshall A, Ni H (2015) Platelets in hemostasis and thrombosis: Novel mechanisms of fibrinogen-independent platelet aggregation and fibronectinmediated protein wave of hemostasis. J Biomed Res 29(6). https://doi.org/10.7555/jbr.29.20150121
66. Hu JT, Lin J, Zhang YY, Lin ZK, Qiao ZW, Liu ZL, Yang W, Liu XG, Dong MY, Guo ZH (2019) A new anti-biofilm strategy of enabling arbitrary surfaces of materials and devices with robust bacterial anti-adhesion via a spraying modified microsphere method. J Mater Chem A 7:26039–26052. https://doi.org/10.1039/c9ta07236e
67. Lin J, Li J, Feng S, Gu C, Li H, Lu H, Hu F, Pan D, Xu BB, Guo Z (2022) An active bacterial anti-adhesion strategy based on directional transportation of bacterial droplets driven by triboelectric nanogenerators. Nano Res. https://doi.org/10.1007/s12274-022-5177-6